JSR Publications

Available Online

J. Sci. Res. **18** (1), 147-165 (2026)

JOURNAL OF SCIENTIFIC RESEARCH

www.banglajol.info/index.php/JSR

Computational Analysis of Tetragonal ThH_2 Hydride: Structural, Electronic, Mechanical, Thermodynamic, and Hydrogen Storage Capabilities for Future Energy Applications

M. M. Islam, H. Mikat, M. Islam*

Nuclear Safety, Security and Safeguard Division, Bangladesh Atomic Energy Regulatory Authority (BAERA), E-12/A, Agargaon, Dhaka-1207, Bangladesh

Received 13 August 2025, accepted in final revised form 28 October 2025

Abstract

In this study, a comprehensive first-principles investigation has been carried out on ThH_2 to evaluate its structural, electronic, elastic, phonon, thermodynamic, and hydrogen storage properties. The calculations were performed using DFT within the framework of the GGA-PBE approximation, employing the CASTEP module. Structural optimization confirmed that ThH_2 crystallizes in a bct phase with space group I4/mmm, and the lattice parameters show good agreement with available experimental and computational data. Electronic band structure and DOS analyses reveal metallic behavior, with significant hybridization between Th-6d and H-1s orbitals. The elastic constants satisfy the mechanical stability criteria and indicate that ThH_2 is ductile and elastically anisotropic. Phonon dispersion confirms the dynamical stability of the compound, with no imaginary frequencies across the Brillouin zone. Temperature-dependent thermodynamic properties such as Debye temperature, Helmholtz free energy, entropy, enthalpy, and heat capacity were also evaluated using the quasi-harmonic approximation. The volumetric hydrogen storage capacity of ThH_2 (82.57 kg/m^3) significantly exceeds the U.S. DOE's 2025 target of 40 kg H_2/m^3, demonstrating its strong potential to meet and surpass future storage requirements. The findings establish ThH_2 as a thermodynamically stable and mechanically robust material, making it a promising candidate for applications in advanced nuclear fuel systems and storage technologies.

Keywords: Tetragonal ThH_2; DFT; Thermodynamics; Hydrogen storage.

doi: https://dx.doi.org/10.3329/jsr.v18i1.83725 J. Sci. Res. **18** (1), 147-165 (2026)

1. Introduction

Metal hydrides are increasingly recognized for their crucial role in advanced technological fields, owing to their outstanding ability to store hydrogen, excellent corrosion resistance, and remarkable stability at elevated temperatures [1]. Thorium and its compounds have garnered significant research interest due to their exceptional physical properties and potential applications in both next-generation nuclear reactors operating within a closed fuel cycle-offering enhanced safety features-and hydrogen storage systems.

*Corresponding author: m.islam4399@gmail.com

In particular, thorium hydride (ThH_2) has emerged as a promising candidate for use in advanced nuclear fuel systems, owing to its unique combination of thorium's fertile nuclear characteristics and the favorable thermal and hydrogen-related properties of metal hydrides. The presence of hydrogen enables effective neutron moderation, facilitating an optimal neutron economy with a reduced volume of coolant. Moreover, ThH_2 offers a higher heavy metal density compared to conventional oxide fuels, which is advantageous for compact reactor core configurations. Its high hydrogen-to-metal ratio makes it a dense hydrogen carrier, essential for enhancing both neutron moderation and heat transfer. In addition, ThH_2 exhibits excellent thermal conductivity, structural integrity, and chemical stability at elevated temperatures, making it well-suited for the demanding conditions encountered in nuclear reactor environments.

Its relatively low neutron absorption cross-section and the ability to breed fissile uranium-233 through neutron capture make ThH_2 particularly attractive in thorium-based fuel cycles, such as in molten salt reactors (MSRs), gas-cooled fast reactors (GFRs), and accelerator-driven systems (ADS). These properties also support its use in solid-state hydrogen storage, tritium breeding in fusion technology, and high-temperature thermochemical processes. Furthermore, the polymorphic nature of ThH_2 offers additional flexibility in tailoring its properties for specific technological needs. ThH_2 exists in multiple polymorphic forms, including the cubic (CaF_2-type) [2] and tetragonal ($PbCl_2$-type) structures, each exhibiting distinct structural and functional behaviors. The metallic conductivity, radiation tolerance, and structural adaptability of ThH_2 make it a multifunctional candidate material not only for safe and efficient nuclear fuel applications but also for broader uses in hydrogen economy infrastructure and other emerging energy systems aimed at achieving sustainability and carbon neutrality. Beyond nuclear applications, hydrogen-rich metal hydrides are also of growing interest for their potential in superconductivity research. This dual significance of thorium hydrides-in both nuclear and condensed matter physics-highlights their importance in the development of advanced functional materials.

Since previous studies by Liu *et al.* [3] and Wang *et al.* [4] revealed that the cubic phase of ThH_2 is dynamically unstable, and Wang *et al.* [4] further confirmed its mechanical instability, the tetragonal phase of ThH_2 has been selected for investigation in the current study. Wang *et al.* [4] studied the electronic, elastic, and phonon dynamical properties of tetragonal ThH_2, while Shein *et al.* [5] investigated its electronic structure. Additionally, the experimental structural parameters were obtained from previous research [6,7]. In our earlier investigation, tetragonal XH_2 (X = Y, Zr) exhibited superior stability and physical performance compared to their cubic counterparts. Following this trend, tetragonal ThH_2 has been selected for a detailed computational study in the present work.

First-principles density functional theory (DFT) provides a robust framework for understanding and predicting the fundamental properties of ThH_2 polymorphs at the atomic scale. This computational approach allows detailed examination of structural, mechanical, electronic, thermodynamic, and phonon dynamical properties without the challenges of handling radioactive materials experimentally. Through DFT-based simulations, it is

possible to evaluate phase stability, bonding characteristics, elastic behavior, and electronic structures, all of which are critical for designing materials for safe and efficient reactor environments. Moreover, such theoretical insights not only help in validating experimental observations but also guide the development and optimization of advanced materials for nuclear fuel and hydrogen storage applications with improved performance and reliability.

In the present work, DFT-based first-principles simulations are employed to explore the structural, elastic, mechanical, electronic, thermodynamic, and hydrogen storage properties of tetragonal ThH_2. Our study demonstrates that the tetragonal phase of ThH_2 exhibits superior mechanical strength, greater thermodynamic resilience, and enhanced vibrational stability when compared to its cubic counterpart, underscoring its potential for deployment in extreme environments involving high radiation and temperature. Analysis of the electronic band structure and density of states (DOS) reveals its metallic behavior, characterized by a zero bandgap and the absence of magnetic ordering. The lack of localized magnetic moments contributes positively to its structural integrity under irradiation, making it highly compatible with the demands of nuclear applications. Phonon dispersion results further affirm the dynamical stability of the tetragonal structure, bolstering its suitability as a reliable candidate for next-generation energy materials. Additionally, thermodynamic evaluations indicate a higher Debye temperature, elevated melting point, reduced temperature-dependent entropy, and more favorable Helmholtz free energy, all pointing toward exceptional thermal endurance. From a functional standpoint, tetragonal ThH_2 not only delivers more potent mechanical properties but also achieves a higher volumetric hydrogen storage capacity.

This first-principles investigation provides comprehensive insights into the intrinsic properties of tetragonal ThH_2, offering computational guidance for experimental synthesis and supporting its potential integration into advanced nuclear fuel systems and hydrogen-based energy technologies. Although this study is purely computational, it is important to note that thorium is radioactive and requires careful handling in practical applications. Any experimental synthesis or deployment of ThH_2 must follow strict safety protocols, including controlled laboratory environments, personal protective equipment, proper storage, and monitoring of radiation exposure. Moreover, its use in nuclear or industrial systems is subject to regulatory frameworks and licensing requirements, such as those outlined by the International Atomic Energy Agency (IAEA). Awareness of these safety and policy considerations is essential when translating computational insights into real-world applications.

2. Computational Approach

To ensure precise evaluation of the electronic structure and total energy, first-principles calculations were performed using spin-polarized DFT within the Generalized Gradient Approximation (GGA) framework, employing the Perdew-Burke-Ernzerhof (PBE) exchange-correlation functional. The GGA-PBE framework is widely employed for metallic systems as it offers a good balance between computational efficiency and

predictive accuracy. Unlike hybrid functionals, which are more suitable for semiconductors due to their improved treatment of bandgaps, GGA-PBE provides reliable estimates for metallic bonding, structural parameters, and total energies without significant computational cost [8,9]. All computational simulations were performed using the CASTEP module integrated in Materials Studio (version 8.0), which provides a robust platform for predicting the fundamental physical behavior of materials with high reliability [10]. In this study, the interaction between valence electrons and ionic cores was modelled using Vanderbilt-type ultrasoft pseudopotentials [11], which allow for accurate and efficient representation of electron-ion interactions in plane-wave-based calculations. For electronic structure calculations, the electronic minimization followed the density mixing scheme. The plane-wave cutoff energy was set to 450 eV to maintain computational accuracy (Table 1), and Structural optimization was performed until strict convergence thresholds were met, specifically 5×10^{-6} eV/atom for total energy, 0.01 eV/Å for maximum force, 0.02 GPa for maximum stress, and 5×10^{-4} Å for maximum atomic displacement. Brillouin zone integration was executed using a 9×9×7 Monkhorst-Pack *k*-point mesh for ThH_2 [12]. Structural optimization of the system to its ground-state configuration was carried out employing the Broyden-Fletcher-Goldfarb-Shanno (BFGS) minimization algorithm [13]. For pseudopotential generation, the valence electron configurations were defined as Th ($6s^2$ $6p^6$ $6d^2$ $7s^2$) and H ($1s^1$). This comprehensive computational methodology ensures accurate and predictive insights into the intrinsic physical properties of ThH_2, thereby establishing its potential as a promising candidate for advanced functional materials.

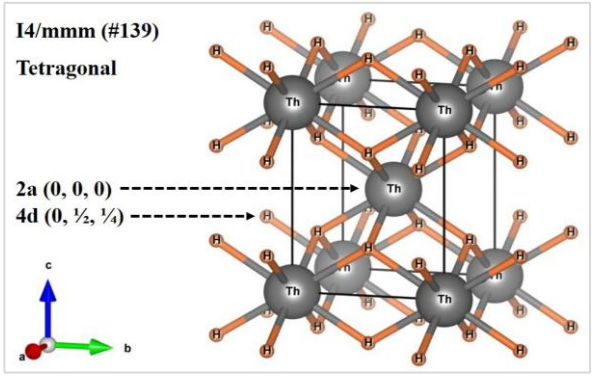

Fig. 1. Schematic 3D crystal structure of tetragonal ThH_2.

The elastic stiffness constants (C_{ij}) were calculated using the finite strain theory approach, as implemented in the CASTEP simulation package [14]. To visualize the fully relaxed three-dimensional (3D) crystal structure, the VESTA software was employed [15], facilitating a clear representation of the atomic arrangement. Furthermore, to analyze the elastic anisotropy of the material, the ELATE online tool was utilized [16]. This tool enabled the generation of 3D plots for Young's modulus, shear modulus, and Poisson's ratio, thereby providing detailed insight into the directional dependence of the material's elastic behavior.

Table 1. Geometrically relaxed unit cell parameters of ThH_2 compared with other tetragonal hydrides.

Compound	Method	Simulation package	Cut-off energy (eV)	k-point grid	Lattice constant (Å) a	Lattice constant (Å) c	c/a	Volume, V (Å)^3	Formation energy, E_f (eV/atom)	Remarks
ThH_2	GGA-PBE	CASTEP	450	9×9×7	4.019	5.013	1.25	80.965	−173.223	This work
	GGA	VASP	450	9×9×9	4.0670	4.9125	-	-	-	[3]
	GGA-PBE	WIEN2k	-	-	4.0475	4.9778	-	-	-	[4]
	Experiment	-	-	-	4.10	5.03	1.23	-	-	[5,6]
YH_2	GGA-PBE	CASTEP	650	10×10×8	3.734	5.294	1.42	73.818	−79.989	[1]
ZrH_2	GGA-PBE	CASTEP	650	10×10×8	3.530	4.426	1.25	55.156	−443.464	[1]

Table 2. Electronic and magnetic parameters of tetragonal ThH_2, YH_2, and ZrH_2.

Compound	Method	Bandgap, E_g (eV)	Electronic property	No. of atoms per unit cell	No. of formula units (f.u.) per unit cell	Magnetic moment, μ_{total} (μ_B/f.u.)	Remarks
ThH_2	GGA-PBE	0.00	Metallic	6	2	0.00	This
YH_2	GGA-PBE	0.00	Metallic	6	2	0.00	[1]
ZrH_2	GGA-PBE	0.00	Metallic	6	2	0.00	[1]

3. Results and Discussion

3.1. *Structural study*

Fig. 1 illustrates the 3D representation of the tetragonal crystal structure of ThH_2 metal hydrides, clearly depicting the space group symmetry and the specific crystallographic sites occupied by the constituent atoms. The structural characteristics of tetragonal ThH_2 have been systematically investigated based on geometry-optimized configurations obtained from first-principles calculations. Table 1 summarizes the optimized lattice parameters and atomic positions and includes a comparison with relevant data reported in the literature, thereby validating the accuracy and reliability of the present computational approach. At standard ambient conditions, thorium dihydride crystallizes in a body-centered tetragonal (bct) ionic structure, categorized under space group I4/mmm (No. 139). In Wyckoff notation, thorium atoms occupy the 2a (0, 0, 0) positions. In contrast, hydrogen atoms are located at the 4d (0, 0.5, 0.25) sites, as illustrated in Fig. 1. The optimized lattice parameters were found to be a = 4.019 Å and c = 5.013 Å, showing reasonable agreement with both theoretical and experimental values [3-6]. The deviations from the experimental lattice constants were 1.97 % for a and 0.34 % for c, demonstrating the high accuracy of the present calculation [5]. Yields a c/a ratio of approximately 1.25, signifying a considerable elongation along the c-axis in comparison to the basal plane. Such a value indicates notable tetragonal distortion, which can influence various physical properties, including elastic behavior, charge distribution, and bonding characteristics. The calculated equilibrium volume for the bct phase was 40.68 Å^3.

The thermodynamic stability of a compound can be evaluated by calculating its formation energy (E_f). The formation energy of tetragonal ThH_2 is determined using the following relation [1,17]:

$$E_f(ThH_2) = \frac{E(ThH_2) - E(Th) - 2E(H)}{N},$$

where E(Th) and E(H) denote the total energies of isolated thorium and hydrogen atoms, respectively, while E(ThH_2) corresponds to the total energy of the ThH_2 unit cell, here, N denotes the total number of atoms in the unit cell, which is 6 for ThH_2. Each unit cell consists of 2 thorium (Th) atoms and 4 hydrogen (H) atoms, corresponding to 2 formula units (ThH_2) per unit cell, listed in Table 2. This atomic configuration is consistent with the crystallographic data of the body-centered tetragonal structure and plays a crucial role in determining the material's physical and thermodynamic properties. Our earlier published work revealed that YH_2 and ZrH_2 both adopt the same stable tetragonal structure, containing two formula units within each unit cell [1]. The computed value of formation energy is −173.223 eV/atom, presented in Table 1. A compound is considered thermodynamically stable if its formation energy is negative [1,17,18]. As shown in Table 1, the negative value of (E_f) confirms the thermodynamic stability of the ThH_2 compound under investigation.

3.2. *Phonon dynamics*

The phonon energy dispersion offers critical insights into the dynamical behavior of materials. It plays a vital role in the evaluation of thermophysical properties such as specific heat, sound velocity, thermal expansion, heat conduction, vibrational entropy, and free energy, particularly through the quasi-harmonic approximation. In the present study, phonon dispersion curves (PDC) are presented only for the structure found to be dynamically stable [1,17,18]. The phonon dispersion curve and the corresponding phonon density of states (PHDOS) for ThH_2 have been computed at zero pressure and temperature by tracing the vibrational frequencies along selected high-symmetry directions, as illustrated in Fig. 2. A detailed analysis of the PDC and PHDOS, as shown in Fig. 2, reveals that the phonon modes are distributed in two distinct frequency regions. Given that the primitive unit cell of ThH_2 contains six atoms (Fig. 1), there are a total of 18 vibrational modes, comprising 3 acoustic and 15 optical modes. The acoustic modes, often associated with structural instabilities and phase transformations, arise primarily from soft vibrational modes. In ThH_2, the lower optical branches overlap with the acoustic branches, indicating no significant gap between them. This overlap suggests interactions between acoustic and low-frequency optical phonons, which can contribute to better thermal transport properties [19]. The dispersion curves exhibit a clear phonon bandgap-approximately 3.8 THz-splitting the optical branch. This gap arises due to the significant mass disparity between thorium and hydrogen atoms, a well-known phenomenon in lattice dynamics. The significant mass difference affects the range of vibrational frequencies for acoustic and optical modes, resulting in a distinct separation between them, as evident in Fig. 2a Importantly, no imaginary frequencies are observed throughout the Brillouin zone,

affirming the dynamical stability of the body-centered tetragonal (bct) phase of ThH_2. The high-frequency optical modes observed in the PDC and PHDOS are predominantly attributed to the light hydrogen atoms, which naturally vibrate at higher frequencies compared to the heavier thorium atoms. This also implies relatively weaker electron–phonon interactions. Furthermore, the PHDOS in Fig. 2b reflects the optical region separated by a phonon bandgap, consistent with the phonon dispersion characteristics.

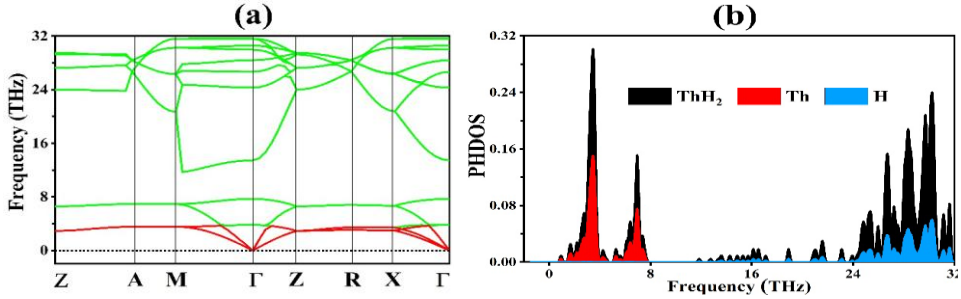

Fig. 2. (a) Phonon dispersion curves (PDC), and (b) phonon density of states (PHDOS) of ThH_2 evaluated by GGA.

3.3. *Band structure*

Let us now look at the details of the electronic structure for ThH_2. The electronic band structure of ThH_2 along high-symmetry directions in the Brillouin zone is depicted in Fig. 3. The Fermi level E_F is set at 0 eV and is marked by the dashed horizontal line. Both spin-up and spin-down states are included in the plot; however, the complete overlap between them confirms the non-magnetic nature of the compound [5,20]. A close inspection of the band structure reveals several bands crossing the Fermi level, a definitive signature of metallic conductivity, which is advantageous for charge transport during hydrogen adsorption and desorption. The conduction and valence bands are continuous across E_F without any bandgap, supporting the conclusion drawn from the total and partial density of states (TDOS and PDOS) analysis presented in Fig. 4. The dispersion of bands around the Fermi level, particularly in the vicinity of the Γ and R points, indicates the availability of partially filled electronic states that contribute to electrical conductivity. The band structure also displays moderate dispersion near the Fermi level, suggesting the presence of delocalized electronic states, which enhance the material's electronic mobility. The bands located deep in the valence band region (-7 to -3 eV) are relatively flat, indicative of localized bonding states, primarily associated with hydrogen orbitals. In contrast, the conduction bands are largely influenced by Th-6d orbitals, as confirmed by the PDOS analysis. No band splitting is observed between the spin channels, implying that ThH_2 remains in a spin-degenerate and non-magnetic ground state, consistent with the symmetric PDOS shown later. Overall, the calculated band structure complements the DOS analysis, reaffirming the metallic character and electronic stability of ThH_2 in its tetragonal phase.

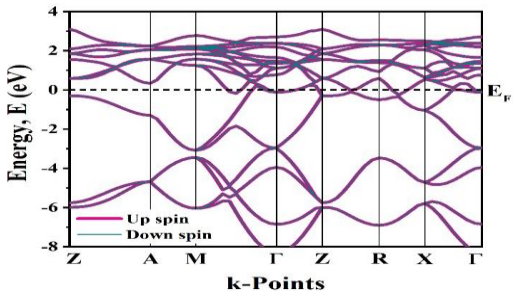

Fig. 3. Energy band diagram of tetragonal ThH_2 evaluated by GGA functional.

3.4. *Density of states*

To gain deeper insight into the electronic structure of ThH_2, the total density of states (TDOS) and partial density of states (PDOS) were calculated, and the results are illustrated in Fig. 4. Fig. 4(a) displays the TDOS of ThH_2 over the energy range from -8 eV to +4 eV, with the Fermi level (E_F) set at 0 eV. The presence of a finite DOS of states at E_F confirms the metallic nature of ThH_2. The states just below and above the Fermi level are predominantly occupied, indicating a substantial degree of electronic delocalization. Multiple sharp peaks appear in the conduction band region, particularly between 1-3 eV, reflecting the availability of several unoccupied states contributing to electrical conductivity. The relatively high TDOS values (2.11 electrons/eV) at the E_F suggest considerable metallic character and enhanced carrier mobility in the system. Fig. 4b presents the spin-polarized PDOS for ThH_2, showing the contributions from Th (orange curve) and H (red curve) atoms. The electronic states near the Fermi level are dominated mainly by Th-6d orbitals, with minor contributions from H-1s orbitals. The hydrogen-derived states are primarily located in the deeper energy range (-7 to -3 eV), indicating strong hybridization with thorium states in the valence band. This orbital overlap suggests covalent character in the Th-H bonding, in addition to the expected ionic interaction. The conduction band is mainly formed by Th-6d states, which confirms the role of thorium in contributing to the compound's electrical conductivity. Moreover, the near symmetry of spin-up and spin-down states in the PDOS plot indicates the non-magnetic nature of ThH_2 [21]. No spin splitting is observed, confirming that the ground state of the material is spin-degenerate. These findings are consistent with previous experimental and theoretical studies [2-7], validating the computational approach adopted in this work. The detailed analysis of TDOS and PDOS thus provides a comprehensive understanding of the electronic origin of the bonding, conduction, and stability in ThH_2.

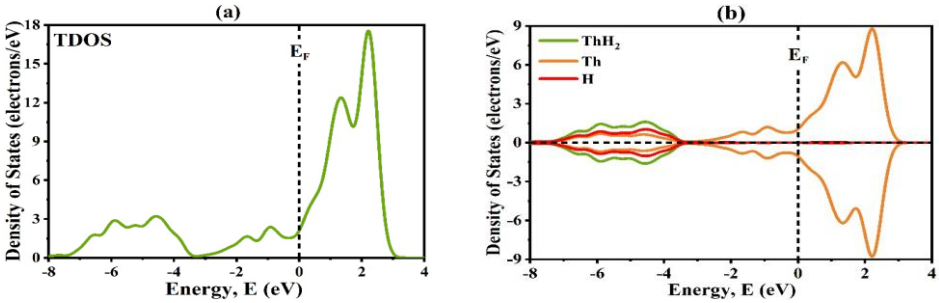

Fig. 4. The (a) total DOS, and (b) partial DOS of ThH_2 hydride.

3.5. *Elastic constants calculations*

The computed elastic stiffness constants (C_{ij}) for ThH_2 are presented in Table 3, along with comparative values for ThH_2 from literature [4] and for isostructural metal hydrides YH_2 and ZrH_2 [1]. The calculated elastic constants exhibit a close correspondence with the theoretical results reported by Wang *et al.* [4]. Minor discrepancies between the present values and those in the literature are primarily due to differences in the computational methodologies and parameter settings. While, Wang *et al.* performed their calculations using the Vienna *ab initio* Simulation Package (VASP), the present study employed the CASTEP code to determine the elastic constants. Since experimental measurements for the elastic properties of tetragonal ThH_2 are not yet available, direct comparison with experimental data could not be made. Nevertheless, the close alignment of our results with previous theoretical reports validates the robustness and accuracy of the current DFT-based investigation.

The six independent elastic constants- C_{11}, C_{12}, C_{13}, C_{33}, C_{44}, and C_{66}- reflect the mechanical response of the tetragonal crystal under different modes of deformation. The relatively high values of C_{11} (170.81 GPa) and C_{12} (106.12 GPa) indicate significant resistance to longitudinal and transverse strains in the a–b plane, respectively. Notably, C_{11} is higher than the corresponding value reported in reference [4], suggesting improved elastic stiffness along the principal crystallographic axes in the present calculations. The C_{13} and C_{33} values reflect the material's stiffness along the c-axis, with C_{33} slightly higher than C_{13}, implying mild anisotropy in axial deformation. A substantial increase in C_{44} (69.92 GPa) compared to previous data (29 GPa) [4] demonstrates improved resistance to shear deformation in planes perpendicular to the c-axis. However, C_{66} remains relatively low (5.14 GPa), indicating a softer shear response along the a–b plane, which may influence the mechanical anisotropy of the system. Table 3 reveals that tetragonal ThH_2 meets the mechanical stability criteria [12], where conditions such as $C_{11}>|C_{12}|$, $2C_{13}^2<C_{33}(C_{11}+C_{12})$, $C_{44}>0$, and $C_{66}>0$ are satisfied. The Cauchy pressure (C_P'), determined by the calculated elastic constants, serves as an indicator of a material's ductile or brittle nature. For tetragonal and hexagonal symmetry, it is calculated as $C_{P1}' = C_{13}-C_{44}$ and $C_{P2}' = C_{12}-C_{66}$ [1,22,23]. Brittle materials exhibit negative values for C_P' (i.e., $C_P'< 0$). Analyzing the value listed in

Table 3, it is decided that ThH_2 exhibits mechanical ductility. This conclusion is based on the understanding that a positive C_P value signifies ductility, whereas a negative value indicates brittleness. The tetragonal shear modulus, denoted as C′, serves as an indicator of the material's overall stiffness and can be determined using the formula $C' = \frac{C_{11}-C_{12}}{2}$. A positive tetragonal shear modulus implies dynamic stability within the solid [22-24]. Therefore, the examined tetragonal ThH_2 phase exhibits dynamical stability, as indicated in Table 3. When compared to other hydrides such as YH_2 and ZrH_2, ThH_2 exhibits intermediate stiffness. Overall, the elastic constants confirm that ThH_2 is mechanically stable and moderately anisotropic, with distinct shear and axial responses that may influence its potential applications in structural or energy-related environments.

Table 3. Elastic stiffness constants (C_{ij}), Cauchy pressure (C_P'), and tetragonal shear modulus (C′) of tetragonal hydrides.

Properties	ThH_2	ThH_2 [4]	YH_2 [1]	ZrH_2 [1]
C_{11} (GPa)	170.81	131	186.60	248.35
C_{12} (GPa)	106.12	100	11.87	66.11
C_{13} (GPa)	95.29	78	60.32	105.20
C_{33} (GPa)	95.81	89	139.56	152.46
C_{44} (GPa)	69.92	29	86.89	64.92
C_{66} (GPa)	5.14	5	38.40	5.59
C_{P1}' (GPa)	25.37	-	−26.57	40.28
C_{P2}' (GPa)	100.98	-	−26.53	60.52
C′ (GPa)	32.34	-	-	-

3.6. *Mechanical properties*

Assessment of mechanical parameters such as the bulk modulus (B), shear modulus (G), Young's modulus (Y), Pugh's ratio (B/G), Vickers hardness (H_V), machinability index (B/C_{44}), and Poisson's ratio (σ) is vital for determining a material's suitability in structural and technological applications. To obtain the polycrystalline elastic moduli, the well-established Voigt-Reuss-Hill (VRH) approximation is utilized, wherein the Voigt and Reuss bounds are first calculated from the elastic stiffness constants. These bounds are then averaged to derive the bulk and shear moduli. Subsequently, the Young's modulus and Poisson's ratio are computed using standard relations involving B and G, as reported in references [1,18,24-27]:

$B = \frac{B_V+B_R}{2}$, where $B_V = \frac{2(C_{11}+C_{12})+C_{33}+4C_{13}}{9}$ and $B_R = \frac{(C_{11}+C_{12})C_{33}-2C_{13}^2}{C_{11}+C_{12}+2C_{33}-4C_{13}}$.

B_V and B_R are the Voight and Reuss bulk moduli, respectively.

$G = \frac{G_V+G_R}{2}$, where $G_V = \frac{C_{11}+C_{12}+2C_{33}-4C_{13}+12C_{44}+12C_{66}}{30}$ and

$G_R = \frac{\frac{5}{2}[(C_{11}+C_{12})C_{33}-2C_{13}^2]C_{44}C_{66}}{3B_VC_{44}C_{66}+[(C_{11}+C_{12})C_{33}-2C_{13}^2](C_{44}+C_{66})}$.

The Voigt (G_V) and Reuss (G_R) shear moduli were calculated to evaluate the polycrystalline shear behavior of the material. Using the obtained bulk modulus (B) and average shear modulus (G), the corresponding Young's modulus (Y) and Poisson's ratio

(σ) were subsequently determined by employing the conventional mathematical expressions [1]:

$$Y = \frac{9BG}{3B+G} \text{ and } \sigma = \frac{3B-2G}{2(3B+G)}.$$

The Vickers hardness (H_V) can be determined using the relationship between the values of Y and σ [1]:

$$H_V = \frac{(1-2\sigma)Y}{6(1+\sigma)}.$$

To further characterize the mechanical response of ThH_2, we evaluated the machinability index (B/C_{44}) and Pugh's ratio (B/G) [28], alongside other key mechanical properties. These parameters are summarized in Table 4, offering a comparative insight with previously reported ThH_2 values and other dihydride materials like YH_2 and ZrH_2. The machinability index serves as a practical metric for understanding how readily a material can be shaped or cut in industrial applications. Higher values generally correspond to improved machinability, resulting in reduced tool wear and enhanced production efficiency. For ThH_2, a machinability index of 1.50 was obtained, indicating a favorable machining performance when compared to the lower value of 0.99 for brittle YH_2. In parallel, the Vickers hardness (H_V) reflects the resistance of a material to localized plastic deformation or indentation. ThH_2 exhibits a relatively low H_V of 2.08 GPa, consistent with its ductile behavior. Notably, an inverse trend is typically observed between machinability and hardness; as hardness increases, machinability tends to decline— a trend that holds when comparing ThH_2 to YH_2 (ZrH_2), which shows a significantly higher H_V of 12.30 GPa (2.99 GPa) but a lower machinability index. Poisson's ratio (σ), which represents the ratio of lateral to axial strain, also serves as a mechanical indicator of ductility. A critical threshold of 0.26 is widely used to distinguish between ductile ($\sigma > 0.26$) and brittle ($\sigma < 0.26$) materials [29]. ThH_2 exhibits a Poisson's ratio of 0.383, strongly suggesting ductility. This value also suggests that atomic bonding in ThH_2 is governed by central force interactions, typically associated with values in the range of 0.25 to 0.50. Moreover, comparison with benchmark ionic and covalent materials- where σ is generally around 0.33 for ionic crystals and approximately 0.10 for covalent solids- implies a significant ionic contribution in ThH_2.

Table 4. Elastic moduli (B, G, Y), Pugh's ratio (B/G), Vickers hardness (H_v), machinability index (B/C_{44}) and Poisson's ratio (σ) of tetragonal hydrides.

Properties	ThH_2	ThH_2 [3]	YH_2 [1]	ZrH_2 [1]
B (GPa)	105.17	91	86.42	131.77
G (GPa)	26.62	16	63.00	35.90
Y (GPa)	73.66	44	152.05	98.73
B/G	3.95	-	1.37	3.67
H_v (GPa)	2.08	-	12.30	2.99
B/C_{44}	1.50	-	0.99	2.03
σ	0.383	0.419	0.207	0.375
Stability	Stable	Stable	Stable	Stable
Nature	Ductile	Ductile	Brittle	Ductile

Pugh's ratio, defined as the ratio of bulk modulus to shear modulus (B/G), offers another perspective on ductility. For ThH_2, a B/G value of 3.95 is calculated, well above the ductility

threshold of 1.75. This finding aligns with the interpretation of Poisson's ratio, reinforcing the ductile nature of ThH_2. Collectively, the mechanical property profile of ThH_2 suggests a material that is structurally stable, soft, and highly machinable, with strong potential for applications where formability and ductility are essential. These results are also in agreement with earlier findings reported by Islam *et al.* [1].

3.7. *Anisotropy*

Elastic anisotropy characterizes the variation of elastic properties with crystallographic direction, whereas isotropy denotes uniform mechanical behavior in all directions. In isotropic materials, elastic constants remain consistent irrespective of orientation; however, in anisotropic materials, these properties vary with direction. The presence of anisotropy plays a pivotal role in diverse scientific and engineering applications, including materials design, structural analysis, and geomechanics. For anisotropic systems, especially in crystalline solids, accurately assessing directional elastic responses is vital for predicting performance under complex loading conditions. In this context, the present investigation examines the anisotropic nature of tetragonal ThH_2, employing key parameters such as the Zener anisotropy index and related elastic anisotropy factors to quantitatively describe the directional dependence of its mechanical behavior using the following equations [1,17,18,30].

Zener anisotropy index, $A = \frac{2C_{44}}{C_{11}-C_{12}}$, bulk anisotropy index, $A^B = \frac{B_v-B_R}{B_v+B_R}$, shear anisotropy index, $A^G = \frac{G_v-G_R}{2G_H}$, and universal anisotropy index, $A^U = 5\frac{G_v}{G_R} + \frac{B_v}{B_R} - 6$.

A material is deemed isotropic when its Zener anisotropy index equals unity (A = 1), and the bulk, shear, and universal anisotropy indices approach zero ($A^B = A^G = A^U = 0$) [18,22]. These criteria signify uniform elastic behavior in all directions. However, the analysis of the calculated values presented in Table 5 indicates that the Zener anisotropy index, shear anisotropy index, and universal anisotropy index all exceed their respective critical thresholds. This deviation demonstrates that the investigated compound exhibits pronounced elastic anisotropy, confirming its inherent directional dependence in mechanical response.

Table 5. Anisotropy factors of tetragonal ThH_2 compound.

Properties	Tetragonal ThH_2
A	2.16
A^B	0.09
A^G	0.44
A^U	8.09

A comprehensive understanding of directional mechanical behavior can be effectively obtained through two-dimensional (2D) and 3D contour plots, which serve as powerful tools for visualizing elastic anisotropy or isotropy. These graphical representations enhance interpretability by highlighting directional variations in elastic properties. In the present

study, the ELATE tool [16,31] has been employed to generate 2D and 3D plots of Young's modulus (Y), shear modulus (G), and Poisson's ratio (σ) for tetragonal ThH_2, as shown in Fig. 5. The observed deviations from spherical symmetry in the 3D contours indicate anisotropic behavior, as the values of Y, G, linear compressibility, and σ vary significantly with direction. It confirms the elastic anisotropy of the ThH_2 compound. Furthermore, Table 6 summarizes the minimum and maximum values of these elastic parameters, offering quantitative insight into the extent of anisotropy.

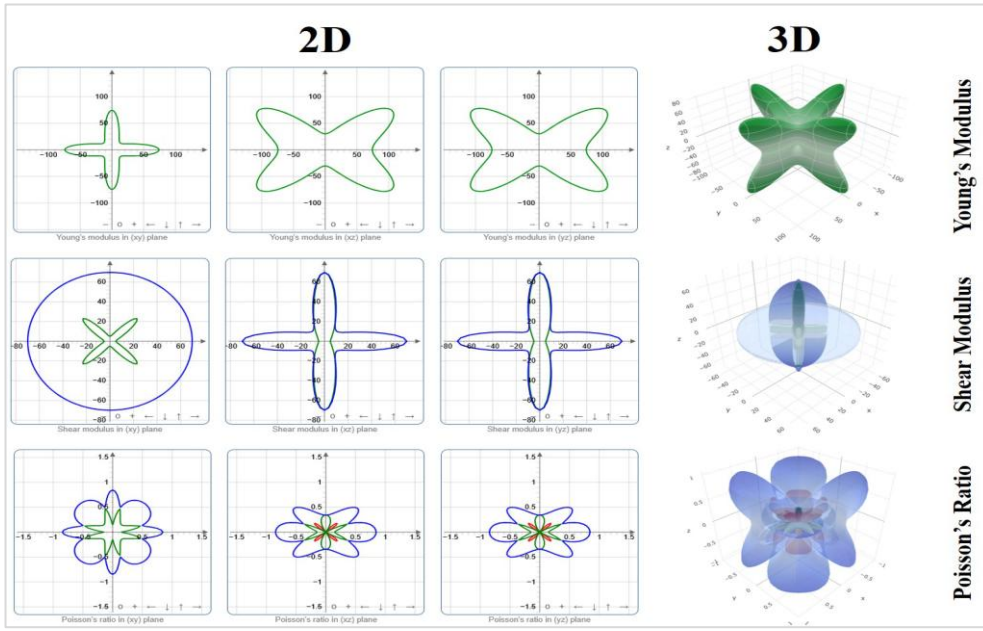

Fig. 5. The anisotropic 3D visualization of Young's modulus, shear modulus, and Poisson's ratio of ThH_2 hydride.

Table 6. The minimum and maximum limit of Young's modulus (Y), shear modulus (G), and Poisson's ratio (σ) of tetragonal ThH_2.

Compound	Young's modulus (GPa)			Shear modulus (GPa)			Poisson's ratio		
	Y_{min}	Y_{max}	Anisotropy	G_{min}	G_{max}	Anisotropy	σ_{min}	σ_{max}	Anisotropy
ThH_2	18.39	128.77	7.00	5.14	69.92	13.61	-0.653	1.376	∞

3.8. *Thermodynamics*

Since thermodynamic properties play an important role in understanding the thermal response of a solid, it is necessary to know the thermal properties of thorium hydrides under high pressures and temperatures. The Debye temperature, Enthalpy, Free energy, entropy, and heat capacity were evaluated by the quasi-harmonic approximation in the temperature range from 0 to 1500 K (Fig. 6).

To gain a deeper understanding of the thermodynamic behavior of ThH_2, temperature-dependent properties such as Debye temperature (θ_D), enthalpy (H), entropy (S), Helmholtz free energy (F), and heat capacity at constant volume (C_V) were calculated within the quasi-harmonic approximation framework. The variations of these parameters with temperature are illustrated in Fig. 6.

As shown in Fig. 6a, where ThH_2 exhibit a sharp drop of θ_D below 80 K, then rapidly increases at lower temperatures before stabilizing at higher temperatures i.e., beyond 600 K, indicating strong interatomic bonding and phonon stiffness. At 300 K, the θ_D for tetragonal ThH_2 is 1240 K, which is slightly lower than that of tetragonal ZrH_2 and YH_2 [1]. At 600 K, the θ_D value for tetragonal ThH_2 increases to 1376 K. This trend arises due to thermal softening of the lattice vibrations at elevated temperatures. A higher θ_D at low temperatures indicates stronger interatomic bonding and higher phonon frequencies, which begin to diminish as temperature rises due to anharmonic effects.

In Fig. 6b, the enthalpy (H) of ThH_2 increases steadily with temperature due to the accumulation of internal energy from lattice vibrations. The observed linearity at elevated temperatures indicates that the compound exhibits stable thermal behavior, thereby making it a suitable candidate for high-temperature applications. This response is typical of crystalline solids, reflecting the transformation of thermal energy into vibrational motion.

Fig. 6c presents the T*entropy curve, which combines temperature and entropy. Entropy increases with temperature, signifying increased atomic disorder. Consequently, the product T*entropy increases more rapidly at higher temperatures, contributing significantly to the total free energy. These findings provide valuable insights into the thermal stability and vibrational behavior of ThH_2, which are crucial for high-temperature applications.

In Fig. 6d the free energy (F) is observed to decrease with rising temperature. It occurs because the product T*entropy in the free energy equation, $F = E - T*entropy$, becomes increasingly significant as thermal motion intensifies. This indicates that although the thermodynamic stability of ThH_2 slightly decreases with increasing temperature, its overall performance remains promising for high-temperature applications. Furthermore, the inclusion of zero-point energy (ZPE)-calculated to be 0.7391 eV for ThH_2-reveals a significant intrinsic energy contribution at 0 K. This underscores the compound's thermodynamic robustness at low temperatures, reinforcing its potential as a stable material under diverse thermal conditions.

Finally, heat capacity at constant volume (C_V), shown in Fig. 6e, exhibits a rapid increase at lower temperatures i.e., below 900K and approaches a constant value at higher temperatures, gradually tending towards the classical Dulong-Petit limit (DPL ~34). This saturation behavior aligns well with the expected phonon contribution to heat capacity under the quasi-harmonic approximation. Notably, ThH_2 exhibits a consistently high heat capacity across the entire temperature range, indicating its strong ability to absorb and retain thermal energy with minimal temperature rise. Such behavior highlights its suitability for applications requiring efficient thermal energy management.

Overall, the thermodynamic curves confirm the thermal stability and predictable vibrational behavior of ThH_2 over a wide temperature range. These insights are essential

for evaluating the compound's potential in temperature-sensitive applications, particularly in nuclear and energy storage systems.

The melting temperature (T_m) of a material is closely associated with its elastic constants, as stronger interatomic forces typically lead to higher melting points. For tetragonal crystal systems, the melting temperature can be estimated using the following empirical relation derived from the elastic constants [1,21,32]:

$$T_m = 354 + 3C_{11} + 1.5C_{33} \pm 300 \text{ K}$$

The calculated melting temperature of tetragonal ThH_2 is 1010 K, which is lower than the estimated values for YH_2 (1123 K) and ZrH_2 (1328 K) [1]. Nevertheless, the overall combination of its physical characteristics positions ThH_2 as a strong candidate for incorporation into next-generation nuclear reactor systems.

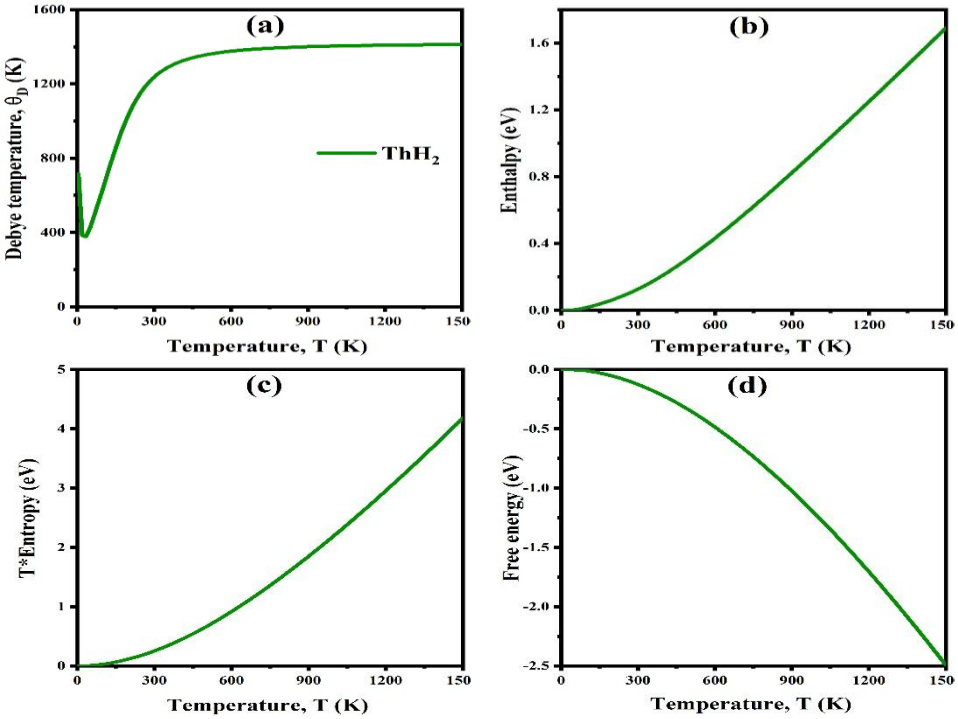

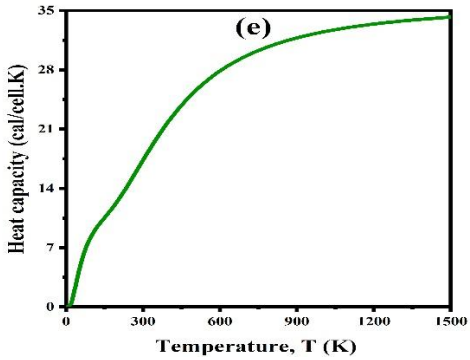

Fig. 6. Temperature-dependent thermodynamic properties of ThH_2: (a) Debye temperature, (b) enthalpy, (c) T*entropy, (d) free energy, and (e) heat capacity.

3.9. *Hydrogen storage capacity*

Calculating the hydrogen storage capacity is vital for assessing and optimizing materials intended for energy storage systems, particularly in the context of fuel cells and clean energy technologies. It serves as a key performance metric, revealing how efficiently a material can store hydrogen either by weight (gravimetric capacity) or by volume (volumetric capacity). This information is essential for the design and development of compact, lightweight, and high-efficiency hydrogen storage devices [1,33-36].

In general, hydrogen storage capacity can be evaluated using two primary methods:

(i) Gravimetric hydrogen storage capacity, which refers to the weight percentage of hydrogen present in the material [1,33-38].

Gravimetric capacity (wt%): $H\ wt\% = \frac{Mass\ of\ H\ atoms}{Molar\ mass\ of\ hydride} \times 100.$

(ii) Volumetric hydrogen storage capacity, which quantifies the amount of hydrogen stored per unit volume of the material [1,36].

Volumetric capacity (kg/m^3): $Volumetric\ H_2 = Density\ of\ hydride \times \left(\frac{H\ wt\%}{100}\right)$

Table 6 presents the hydrogen storage characteristics of tetragonal ThH_2 along with those of several other hydride materials for comparison. The table includes their density, hydrogen content (wt%), and volumetric hydrogen capacity—parameters that are crucial for assessing their potential as solid-state hydrogen storage materials, particularly in nuclear and energy applications. The density of ThH_2 is calculated to be 9601 kg/m^3, which is significantly higher than that of YH_2 (4090 kg/m^3) and ZrH_2 (5614 kg/m^3).

Table 6. Parameters of hydrogen storage capacity.

Compound	Density (kg/m^3)	H (wt%)	Volumetric H_2 (kg/m^3)	Remarks
ThH_2	9601	0.86	82.57	This work
YH_2	4090	2.22	90.80	[1]
ZrH_2	5614	2.16	121.26	[1]
$RbSrH_3$	-	1.71	-	[33]

Rb_2CaCdH_6	-	1.69	-	[33]
$RbTiH_3$	-	2.22	-	[33]
$NaSrH_3$	-	2.6	-	[35]
$KNiH_3$	-	3.005	-	[34]
Na_2LiAlH_6	-	3.42	100.63	[36]
Rb_2SiH_6	-	2.86	-	[37]
TiH_4	-	7.77	-	[38]

However, despite this high density, ThH_2 exhibits a relatively low hydrogen weight percentage (H wt%) of 0.86 %, compared to 2.22 % for YH_2 and 2.16 % for ZrH_2 [1]. The tetragonal phase of ThH_2 also shows a lower H wt% than $RbSrH_3$, Rb_2CaCdH_6, $RbTiH_3$, $NaSrH_3$, $KniH_3$, Na_2LiAlH_6, Rb_2SiH_6, and TiH_4 (Table 6). This lower hydrogen content is primarily attributed to the higher atomic mass of thorium, which reduces the weight fraction of hydrogen in the compound.

In terms of volumetric hydrogen capacity-a more relevant metric for practical storage systems-ThH_2 stores approximately 82.57 kg/m^3 of hydrogen. Although this value is lower than that of YH_2 (90.80 kg/m^3), ZrH_2 (121.26 kg/m^3), and Na_2LiAlH_6 (100.63 kg/m^3) it considerably surpasses the U.S. DOE's 2025 target of 40 kg H_2/m^3, highlighting its potential as a high-density hydrogen storage material and placing it within a promising range, particularly in light of the compound's thermal and mechanical stability. Although tetragonal ThH_2 exceeds the U.S. DOE's 2025 target for volumetric hydrogen storage capacity, its gravimetric capacity remains considerably lower than the DOE benchmark of 5.5 wt% [38]. Hence, tetragonal ThH_2 can be regarded as a material with moderate volumetric efficiency, potentially applicable in high-density or stationary hydrogen storage systems, especially in environments where mechanical robustness and nuclear compatibility are of primary importance.

4. Conclusion

A comprehensive first-principles investigation of tetragonal ThH_2 was performed to examine its fundamental physical properties relevant to nuclear and energy-related applications. The structural analysis verified the stability of the tetragonal I4/mmm phase, with optimum parameters closely aligning with available published theoretical and experimental reports. Studies of the electronic structure showed that thorium and hydrogen states strongly hybridize, which makes the material behave like a metal. The estimated elastic constants fulfilled the Born stability criteria, and the obtained mechanical properties indicated a ductile and anisotropic nature. The phonon dispersion and phonon DOS validated dynamic stability, exhibiting no soft modes throughout the Brillouin zone. Thermodynamic evaluations based on quasi-harmonic approximation indicated consistent patterns in entropy, enthalpy, free energy, and heat capacity, reinforcing the thermal stability of ThH_2. Furthermore, analysis of mechanical moduli and anisotropy indices suggested potential for structural applications under varying thermal and mechanical conditions. ThH_2 exhibits an advantageous combination of structural integrity, thermal stability, and hydrogen-rich properties, which supports its potential as a candidate material

for advanced nuclear fuels and energy storage systems. The volumetric hydrogen storage capacity of tetragonal ThH_2 (82.57 kg/m^3), although lower than that of YH_2 (90.80 kg/m^3) and ZrH_2 (121.26 kg/m^3), exceeds the U.S. DOE 2025 target of 40 kg H_2/m^3, highlighting its potential as a high-density hydrogen storage material. Its thermal and mechanical stability make it suitable for high-density or stationary hydrogen storage, particularly in applications demanding structural strength and nuclear compatibility. In summary, this study establishes a comprehensive theoretical basis highlighting the enhanced stability and potential of tetragonal ThH_2 for advanced nuclear and energy technologies, surpassing the performance of its unstable cubic form and encouraging continued exploration toward sustainable energy advancements.

Acknowledgment

The authors warmly dedicate this research work to their beloved children.

References

1. M. Islam and M. M. Islam, Chem. Phys. **597**, ID 112805 (2025). https://doi.org/10.1016/j.chemphys.2025.112805
2. J. H. Weaver, J. A. Knapp, D. E. Eastman, D. T. Peterson, and C. B. Satterthwaite, Phys. Rev. Lett. **39**, 639 (1977). https://doi.org/10.1103/PhysRevLett.39.639
3. J.-B. Liu, B.-T. Wang, and J.-Q. Liang, Comput. Mater. Sci. **98**, 15 (2015). https://doi.org/10.1016/j.commatsci.2014.10.055
4. B.-T. Wang, P. Zhang, H. Song, H. Shi, D. Li, and W.-D. Li, **401**, 124 (2010). https://doi.org/10.1016/j.jnucmat.2010.04.009
5. I. R. Shein, K. I. Shein, N. I. Medvedeva, and A. L. Ivanovskii, Phys. B: Cond. Matter **389**, 296 (2007). https://doi.org/10.1016/j.physb.2006.07.001
6. C. Keller, Gmelin Handbook of Inorganic and Organometallic Chemistry - 8th Edition, Th. Thorium (System-Nr. 44), ed. K. C. Buschbeck (Springer Berlin Heidelberg, New York, 1978).
7. R. E. Rundle, C. G. Shull, and E. O. Wollan, Acta Crystall. **5**, 22 (1952). https://doi.org/10.1107/S0365110X52000071
8. J. P. Perdew, K. Burke, and M. Ernzerhof, Phys. Rev. Lett. 77, ID 3865 (1996). https://doi.org/10.1103/PhysRevLett.77.3865
9. M. Islam, J. Sci. Res. **15**, 739 (2023). https://doi.org/10.3329/jsr.v15i3.64394
10. S. J. Clark, M. D. Segall, C. J. Pickard, P. J. Hasnip, M. J. Probert, K. Refson, M. C. Payne, ZeitschriftfuerKristallographie **220**, 567 (2005). https://doi.org/10.1524/zkri.220.5.567.65075
11. D. Vanderbilt, Phys. Rev. B **41**, ID 7892 (1990). https://doi.org/10.1103/PhysRevB.41.7892
12. H. J. Monkhorst and J. D. Pack, Phys. Rev. B **13**, ID 5188 (1976). https://doi.org/10.1103/PhysRevB.13.5188
13. T. H. Fischer and J. Almlof, The J. Phys. Chem. **96**, 9768 (1992). https://doi.org/10.1021/j100203a036
14. F. D. Murnaghan, Am. J. Math. **59,** 235 (1937). https://doi.org/10.2307/2371405
15. K. Momma, F. Izumi, J. Appl. Crystal. **44**, 1272 (2011). https://doi.org/10.1107/S0021889811038970
16. R. Gaillac, P. Pullumbi, J. Phys.: Condensed Matter **28**, ID 275201 (2016). https://doi.org/10.1088/0953-8984/28/27/275201
17. M. Islam, Nucl. Mater. Energy **38**, ID 101631 (2024). https://doi.org/10.1016/j.nme.2024.101631

18. R. Ahmed, M. Mahamudujjaman, M. A. Afzal, M. S. Islam, R. S. Islam and S. H. Naqib, J. Mater. Res. Technol. **24**, 4808 (2023). https://doi.org/10.1016/j.jmrt.2023.04.147
19. M. I. Naher, and S. H. Naqib, Res. Phys. **37**, ID 105505 (2022). https://doi.org/10.1016/j.rinp.2022.105505
20. C. Zhang, S.-P. Guo, H. Jiang, G.-H. Zhong, and Y.-H. Su, The J. Phys. Chem. C **119**, 13465 (2015). https://doi.org/10.1021/acs.jpcc.5b03195
21. M. Islam, Chem. Phys. Impact **7**, ID 100310 (2023). https://doi.org/10.1016/j.chphi.2023.100310
22. M. Islam and M. A. R. Sheikh, Nucl. Mater. Energy **41**, ID 101734 (2024). https://doi.org/10.1016/j.nme.2024.101734
23. M. A. Alam, F. Parvin, and S. H. Naqib, Res. Mater. **21**, ID 100500 (2024). https://doi.org/10.1016/j.rinma.2023.100500
24. F. Mouhat and F.-X. Coudert, Phys. Rev. B **90**, ID 224104 (2014). https://doi.org/10.1103/PhysRevB.90.224104
25. W. Voigt, Lehrbuch der Kristallphysik (Textbook of Crystal Physics) ed. B. G. Teubner (Johnson Reprint Corporation, Berlin, Germany, 1928).
26. A. Reuß, J. Appl. Math. Mechanics **9**, 49 (1929). https://doi.org/10.1002/zamm.19290090104
27. R. Hill, Proc. Phys. Soc. A **65**, 349 (1952). https://doi.org/10.1088/0370-1298/65/5/307
28. S. F. Pugh, J. Sci. **45**, 823 (1954). https://doi.org/10.1080/14786440808520496
29. I. N. Frantsevich, F. F. Voronov, and S. A. Bokuta, Elastic Constants and Elastic Moduli of Metals and Insulators: A Handbook, ed. I. N. Frantsevich (Naukova Dumka, Ukraine, 1982).
30. S. I. Ranganathan and M. Ostoja-Starzewski, Phys. Rev. Lett. **101**, ID 055504 (2008). https://doi.org/10.1103/PhysRevLett.101.055504
31. M. Islam and M. M. Islam, Chem. Phys. **600**, ID 112917 (2026). https://doi.org/10.1016/j.chemphys.2025.112917
32. M. E. Fine, L. D. Brown, and H. L. Marcus, Scripta Metallurgica **18**, 951 (1984). https://doi.org/10.1016/0036-9748(84)90267-9
33. M. K. Shahzad, S. Hussain, M. N. Khan, M. J. Aslam, R. M. Mohammed, V. Tirth, H. Alqahtani, A. Algahtani, T. Al-Mughanam, and W. Azeem, Sci. Rep. **14**, 25102 (2024). https://doi.org/10.1038/s41598-024-76062-0
34. M. A. Rehman, J. Fatima, Z. U. Rehman, S. Y. Alomar, M. Sohiab, A. Hamad, Struct. Chem. **36**, 235 (2025). https://doi.org/10.1007/s11224-024-02362-w
35. D. Tufail, U. Ahmed, M. Haleem, B. Amin, M. Shafiq, RSC Adv. **15**, 337 (2025). https://doi.org/10.1039/D4RA05327C
36. Ç. Yamçıçıer and C. Kürkçü, Int. J. Hydrog. Energy **135**, 440 (2025). https://doi.org/10.1016/j.ijhydene.2025.04.445
37. S. Al and Ç. Yamçıçıer, J. Energy Storage **91**, ID 112033 (2024). https://doi.org/10.1016/j.est.2024.112033
38. S. Al, C. Kurkcu, and C. Yamcicier, Int. J. Hydrog. Energy **45**, 30783 (2020). https://doi.org/10.1016/j.ijhydene.2020.08.108